

Tribological behaviors of Ni-modified citric acid carbon quantum dot particles as a green additive in polyethylene glycol

Zhiqiang TU¹, Enzhu HU^{1,*}, Bangbang WANG², Karl D DAVID³, Philipp SEEGER⁴, Martin MONEKE⁴, Ralph STENGLER⁴, Kunhong HU¹, Xianguo HU²

¹ Department of Chemical and Materials Engineering, Hefei University, Hefei 230601, China

² School of Mechanical Engineering, Institute of Tribology, Hefei University of Technology, Hefei 230009, China

³ Department of Mechanical Engineering, School of Engineering, University of Birmingham, Birmingham B15 2TT, United Kingdom

⁴ Darmstadt Institute of Plastics Engineering, University of Applied Sciences Darmstadt, Darmstadt 64295, Germany

Received: 03 September 2018 / Revised: 27 November 2018 / Accepted: 02 January 2019

© The author(s) 2019.

Abstract: A novel green lubricating oil additive (carbon quantum dot (CQD) particle-doped nickel (Ni-CQD)) was synthesized from citric acid and nickel acetate. The effects of CQD and Ni-CQD nanoparticles on the tribological behaviors of polyethylene glycol (PEG200) were investigated under different loads and reciprocation speeds. The results indicate that CQD and Ni-CQD particles can both enhance the lubrication properties of PEG200. However, the Ni-CQD nanoparticles enhanced the lubrication properties more than the plain CQD particles did. The average friction coefficient and wear rate of PEG200 containing 2 wt% Ni-CQDs were reduced by 35.5% and 36.4%, respectively, compared to PEG200 containing pure CQDs under a load of 8 N and reciprocation speed of 25 mm/s over 60 min. The friction and wear mechanisms are attributed to the fact that friction induces the Ni-CQDs to participate in the formation of a tribofilm, resulting in a low friction coefficient and wear rate.

Keywords: friction; dynamics; joint clearance; numerical models; impact; durability

1 Introduction

The fuel energy consumed in combat friction and wear in modern industries amounts to approximately 30%–40%. Thus, numerous scientists have developed lubrication additives and low-friction materials [1–3]. Commercially available lubricant additives such as zinc dialkyl dithiophosphates (ZDDP) and molybdenum dialkyl dithiophosphates, which contain P, Mo, and S, are used as multifunctional additives. These additives have anti-wear, extreme pressure resistant, and antioxidant properties [4–6]. However, traditional lubricant additives are unfit for real-time applications owing to the strict environmental protection regulations [7]. Over the past decade, inorganic nanoparticles such as carbon materials, niobium particles, molybdenum disulfide, and tungsten disulfide have been extensively

applied as lubricants to improve tribological performance of equipment, save fuel energy, and protect equipment [8–10]. Carbon materials, such as fullerene, carbon nanotubes, graphene, and their hybrids and derivatives, have been widely used as solid lubricants or oil additives owing to their unique self-lubricating effects [7, 11–20]. However, the dispersibility of these materials in base oils is poor, thereby limiting their industrial application. Therefore, stable dispersion additives must be fabricated [21, 22] to enhance tribological performance of equipment and to enable their real-time application in industries.

Carbon quantum dots (CQDs, <10 nm), as a novel type of carbon material, have been extensively investigated based on their outstanding optical properties, robust chemical inertness, and good biocompatibility [14, 23–26]. CQDs have small particle size,

* Corresponding author: Enzhu HU, E-mail: huez@hfu.edu.cn

high specific surface area, and controllable functional surfaces [12]. The dispersibility and storage stability of CQDs in lubricants are substantially improved compared to conventional carbon materials. Limited number of CQD materials have been developed for tribological applications through surface functionalization. Shang et al. [23] investigated the tribological behaviors of carbon hybrids containing CQDs and graphene oxide (GO). The excellent tribological performance of the hybrids was attributed to the synergistic effect of the sphere-like CQDs and GO adsorbed on the sliding surfaces such as the surface of steel. Zhang et al. [27] synthesized a novel N/B-codoped nanomaterial (carbon dots/ionic liquid, CD/IL), and found that the anti-wear and friction-reducing properties of polyethylene glycol (PEG) were improved with the addition of CD/IL particles. Ma et al. [28] fabricated novel CQD and IL nanoparticles and discovered that the tribological behavior of these nanoparticles affects the lubrication of PEG, similar to the results found by Zhang [27]. Wang et al. [29] used a one-pot pyrolysis method to synthesize IL (1-aminopropyl-3-methylimidazolium bromide)-capped carbon dot particles. They indicated that the friction and wear mechanisms of composite particles involve the rolling, mending, and polishing of composite particles under friction, resulting in outstanding tribological behaviors in PEG. Ma [26] reported that the tribological properties of CQD/CuS_x nanocomposites, when used as additives, can enhance lubrication and metal-wear surface-repair capabilities. Yu and Jiang et al. [30–33] fabricated graphene–nickel composites in situ by using powder metallurgy, and then investigated their tribological behaviors and mechanisms. They found that the resulting tribofilms are responsible for the self-lubricating properties of the composites.

As implied by the studies above, research on the preparation of CQD-doped Ni and its tribological behaviors is limited.

In this study, novel Ni-CQD nanoparticles were prepared from citric acid through a facile hydrothermal method. Modern analysis technologies and tribological tests were implemented to investigate the morphology, structure, composition, and tribological properties of the Ni-CQDs. This study aims to develop new lubricants and lubricant additives to prolong the service life and reduce the cost of machinery.

2 Experiments

2.1 Materials and sample preparation

Four grams of commercially available hydrated citric acid (C₆H₈O₇·H₂O) were purchased from Jiangsu Qiangsheng Functional Materials Co., Ltd. Commercially available ethylenediamine (C₂H₈N₂) was purchased from Tianjin Baishi Chemistry Co., Ltd. Commercially available nickel acetate was purchased from Tianjin Damao Chemical Co., Ltd. CQD and Ni-CQD particles were prepared from citric acid using a facile hydrothermal method [34].

The citric acid (4.0 g) and ethylenediamine (1.43 mL) were mixed and stirred using a glass rod for 30 min to form a transparent solution. The solution was then transferred to a hydrothermal reaction kettle (HT-50H-316L, Anhui Kemi Co., Ltd.) to react for 5 h at 160 °C. A rotary evaporation device (RE-201D, Gongyi Yuhua Co., Ltd.) was used to remove the reagents and a dialysis bag (retained molecule weight of 1000 Da) was used to remove the ions. The remaining solution was then placed in a freeze dryer (SCIENTZ-12N, Ningbo Scientz Biotechnology Co., Ltd.) for 24 h to obtain high-quality CQDs. Using the same process, 4.0 g of citric acid, 1.43 mL of ethylenediamine, and 0.3 g of nickel acetate were combined to create high-quality Ni-CQDs. Oil samples of 1 wt%, 2 wt%, and 3 wt% CQDs and Ni-CQDs were prepared via simple mechanical mixing and were then treated ultrasonically for 10 min.

2.2 Analysis methods

High-resolution transmission electron microscopy (HRTEM, JEOL model 2010) was used to investigate the morphologies of the CQDs and Ni-CQDs [35]. Fourier transform infrared spectroscopy (FTIR, Nicolet model 6700) was applied to investigate the chemical compositions and surface functional groups of the two nanomaterials [36]. Friction and wear tests were conducted by using a multifunctional reciprocating tribometer (model CFT-1, Zhongke Kaihua Technology Co., Ltd.) with different loads (8 N, 20 N, and 100 N) and reciprocation speeds (200 rpm, 300 rpm, and 400 rpm, amplitude of 5 mm) for 60 min at room temperature (Approximate 25 °C). Commercially available steel balls (GCr15, 10 grade, Chinese standard) with

diameters of 6 mm were used as the stationary upper counterparts for the friction tests. The hardness of the steel balls was in the range of 60 HRC–63 HRC. The lower specimens were steel disks (GCr15) each with a diameter of 28 mm, thickness of 2 mm, and surface roughness of $0.03\ \mu\text{m}$. The hardness of the steel disks was in the range of 50 HRC–60 HRC. A detailed schematic diagram of the tribometer is shown in Fig. 1. Prior to the friction tests, the friction pairs were washed with acetone in an ultrasonic cleaner for 10 min. All friction tests were conducted three times under the same conditions to ensure repeatability and reliability. Next, 3D laser scanning microscopy (mode VK-X100K) was utilized to investigate the wear profiles of the steel balls and disks. A multi-file analyzer was used to calculate the wear scar diameter, wear width, and wear area. The wear rate of the disks was evaluated using the following formula [37]:

$$K_o = (S_a \times A) / L \times N, \quad (1)$$

where K_o is the wear rate (mm^3/Nm), S_a is the wear area (μm^2), A is the amplitude (mm), L is the sliding distance (m), and N is the load (N). The morphologies and element contents of the wear zones on the surfaces of the disks were analyzed using scanning electron microscopy with energy dispersive spectroscopy (SEM/EDS, model JSM-6700F). The element valence states of the wear zones were investigated using X-ray photoelectron spectroscopy (XPS, ESCALAB250,

Thermo). XPS analysis was performed with a monochromatized Al $K\alpha$ source (1486.6 eV) with a pass energy of 40 eV and tilt angle of 90° . The operating voltage was 12.5 kV and the filament current was 16 mA. Internal calibration used the C–C or C–H components of the C1s spectra at a binding energy of 284.6 eV as references [38]. After subtracting the nonlinear background (straight line), the spectra were deconvoluted using a peak fitting software with a Gaussian fitting method. Raman spectroscopy (LabRAM-HR, resolution of $0.6\ \text{cm}^{-1}$ and scanning repeatability of $\pm 0.2\ \text{cm}^{-1}$) was used to investigate the chemical compositions of the wear zones on the disks and to identify the friction and wear mechanisms.

3 Results and discussion

3.1 Characterization of particles

Figure 2 illustrates the HRTEM images of the CQDs and Ni-CQDs. The CQD particles were agglomerated, as shown in Fig. 2(a). The average particle size (APS) of the Ni-CQD particles was approximately 5 nm–10 nm. The dispersion capacities of the two types of nanomaterials were also investigated, as shown in Fig. 2(c). Both types of particles can be uniformly dispersed in PEG. Figure 2(d) shows the results of FTIR analysis. The wavenumber at $3,435\ \text{cm}^{-1}$ is attributed to $-\text{OH}$ stretching vibrations. The peaks at $2,912\ \text{cm}^{-1}$ and $2,848\ \text{cm}^{-1}$ are attributed to $-\text{CH}_3$ and $-\text{C}_2\text{H}_2-$ groups,

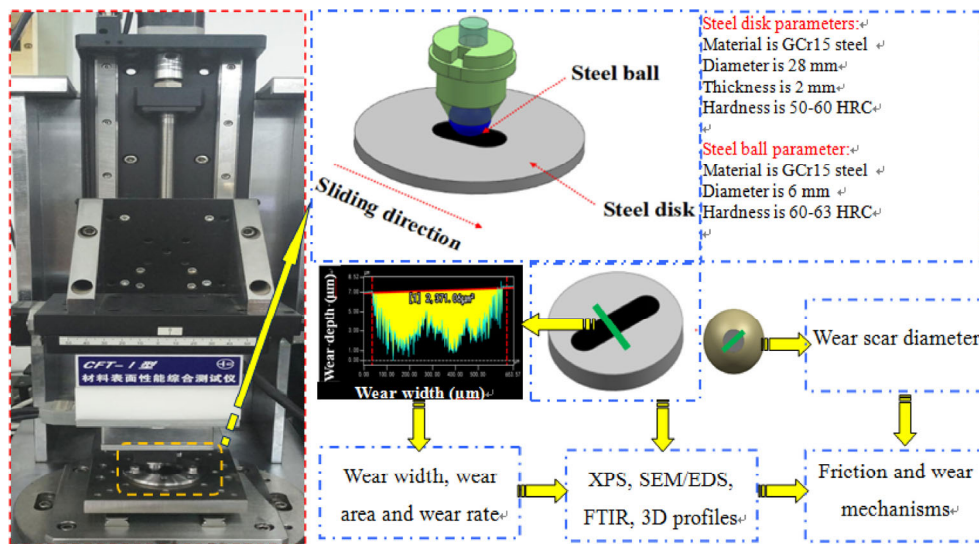


Fig. 1 Schematic diagram of the tribo-meter and analysis methods.

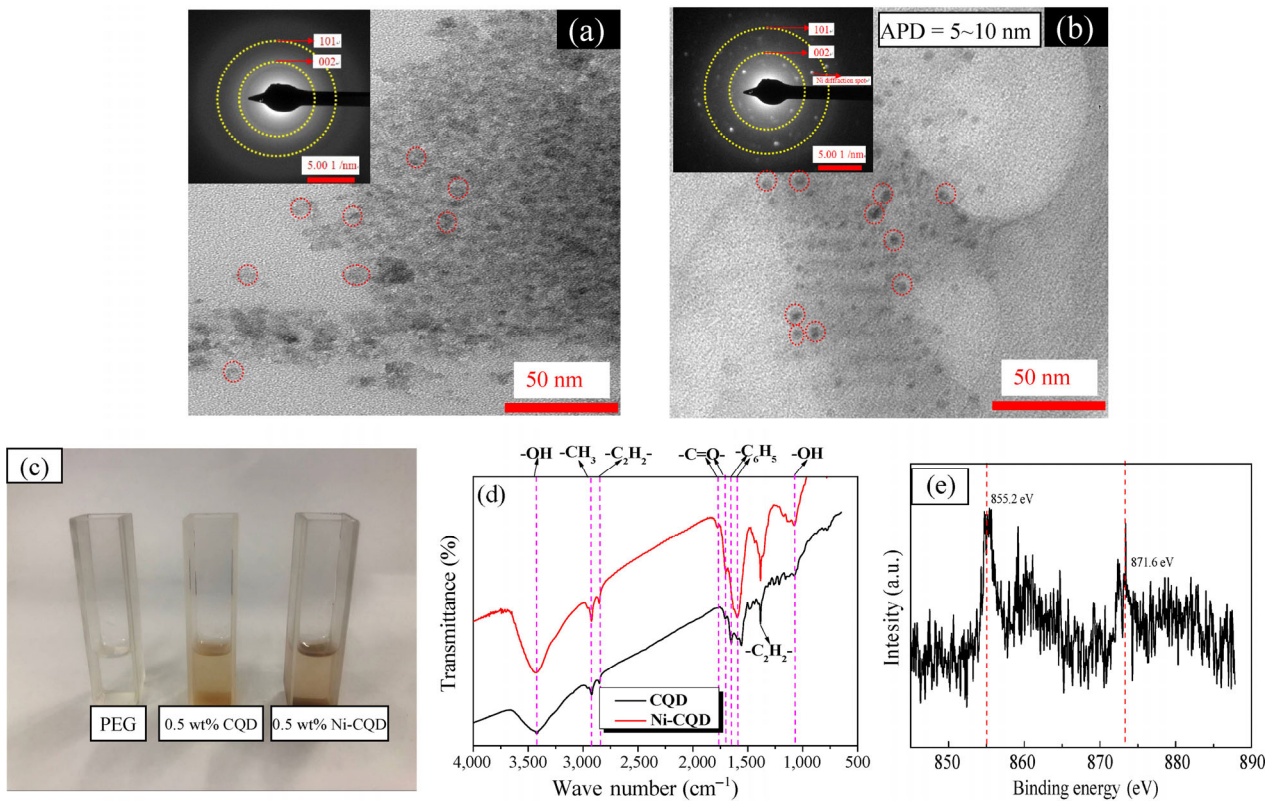


Fig. 2 Characterization of the CQD and Ni-CQD particles (a) HRTEM image and diffraction diagram of the CQD, (b) HRTEM image and diffraction diagram of the Ni-CQD particles, (c) Optical images of 0.5 wt% CQD and Ni-CQD particles in PEG200, (d) FTIR spectra of CQD and Ni-CQD particles, and (e) Ni_{2p} spectrum of Ni-CQD.

respectively. The peaks in the range of $1,702\text{ cm}^{-1}$ – $1,786\text{ cm}^{-1}$ are attributed to C=O groups. The peaks in the range of $1,565\text{ cm}^{-1}$ – $1,643\text{ cm}^{-1}$ are attributed to $-\text{C}_6\text{H}_5$ groups. The peak at $1,079\text{ cm}^{-1}$ is attributed to $-\text{OH}$ bending vibrations. Figure 2(e) presents the Ni_{2p} spectrum analysis of the Ni-CQDs. The peaks at 855.2 eV and 871.6 eV indicate that NiO nanoparticles exist on the surfaces of the CQD particles.

3.2 Friction reduction

Figure 3 presents the variation in the average friction coefficients of PEG200 and the different Ni-CQD particles at different loads with a reciprocation speed of 25 mm/s over 60 min. Figure 3(a) reveals that the Ni-CQD and CQD particles enhanced the lubrication ability of PEG200 under a load of 8 N with a

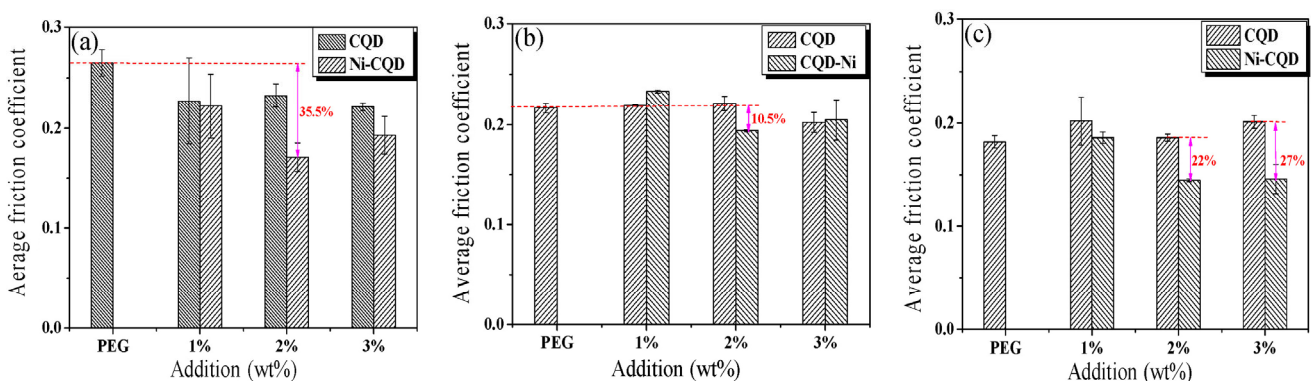


Fig. 3 Variation of average friction coefficient for different oil samples including the 1 wt%, 2 wt% and 3 wt% CQD or Ni-CQD particles at the reciprocation speed of 25 mm/s for 60 min at room temperature conditions under the different loads with: (a) 8 N; (b) 20 N; (c) 100 N.

reciprocation speed of 25 mm/s over 60 min. The average friction coefficient decreased by 35.5% when compared to pure PEG200, when 2 wt% Ni-CQD particles were added to the PEG200. The Ni-CQD particles provided better anti-friction properties to the PEG200 when compared to the plain CQD particles. The results for both types of particles under a 20-N load are presented in Fig. 3(b). The average friction coefficient of the PEG200 with 2 wt% Ni-CQDs was 10.5% smaller than that of the PEG200 with 2 wt% CQDs. The results for both types of particles under 100 N load are presented in Fig. 3(c). Under such a heavy load, the CQD particles could not modify the anti-friction properties of the PEG. However, adding 2 wt% and 3 wt% Ni-CQD particles did modify the anti-friction properties of the PEG. The average friction coefficients for these particle additions decreased by 22% and 27%, respectively. Figure 4 presents the variation in the average friction coefficients with different oil samples under a load of 100 N with different reciprocation speeds over 60 min. The average friction coefficients of the PEG200 with different CQD and Ni-CQD particle contents decreased at the testing conditions of 17 mm/s and 33 mm/s, respectively, when compared to pure PEG200.

In summary, Ni-CQD particles can enhance the anti-friction properties of PEG200 and their efficacy is greater than that of pure CQDs. A typical tendency chart for friction coefficients with different oil samples was used to verify these results, as shown in Figs. 5 and 6.

3.3 Wear resistance

Figure 7 illustrates the variation in the wear rates of

the disks under different loads with a reciprocation speed of 25 mm/s over 60 min. Figure 7(a) illustrates the variation in the wear rates of disks lubricated with different oils under a load of 8 N. The wear rate with the PEG200 containing 1 wt% CQDs decreased by 45.7% when compared to that with the pure PEG200. The wear rate of the disk lubricated with PEG200 containing 1 wt% Ni-CQDs decreased by 88.9%. The wear rates of the disks lubricated with PEG200 containing 2 wt% and 3 wt% CQDs increased due to the aggregation of CQD particles. However, the wear rates of the disks lubricated with PEG200 containing 2 wt% and 3 wt% Ni-CQDs decreased by 36.4% and 23.7%, respectively. These results indicate that the Ni-CQD particles provided better anti-wear properties than the CQD particles. Figure 7(b) illustrates the variation in the wear rates of disks lubricated with different oil samples under a load of 20 N. The wear rates of the disks with PEG200 containing 1 wt% CQDs and 1 wt% Ni-CQDs decreased by 40.8% and 11.1%, respectively, compared to those of the disks with pure PEG200. The wear rates with PEG200 containing 2 wt% and 3 wt% Ni-CQDs decreased by 24.6% and 60.7%, respectively. Figure 7(c) illustrates the variation in the wear rates of the disks lubricated with different oil samples under a load of 100 N. The wear rates of the disks lubricated with PEG200 containing 2 wt% and 3 wt% Ni-CQD particles decreased by 46% and 74.8%, respectively, compared to those of the disks lubricated with pure PEG200. Figure 8 illustrates the variation in wear rates for different oil samples under a load of 100 N with different reciprocation speeds over 60 min. The wear rates with PEG200 containing different amounts of CQD and Ni-CQD particles decreased when

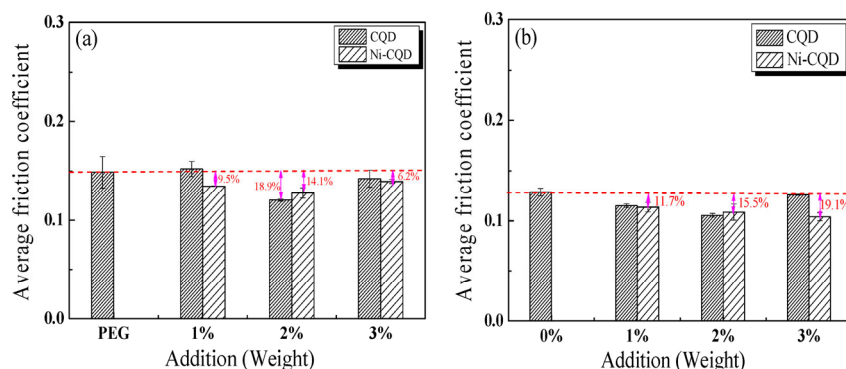


Fig. 4 Variation of average friction coefficient for different oil samples including the 1 wt%, 2 wt% and 3 wt% CQD or Ni-CQD particles at the load of 100 N for 60 min at room temperature conditions under different reciprocation speeds: (a) 17 mm/s; (b) 33 mm/s.

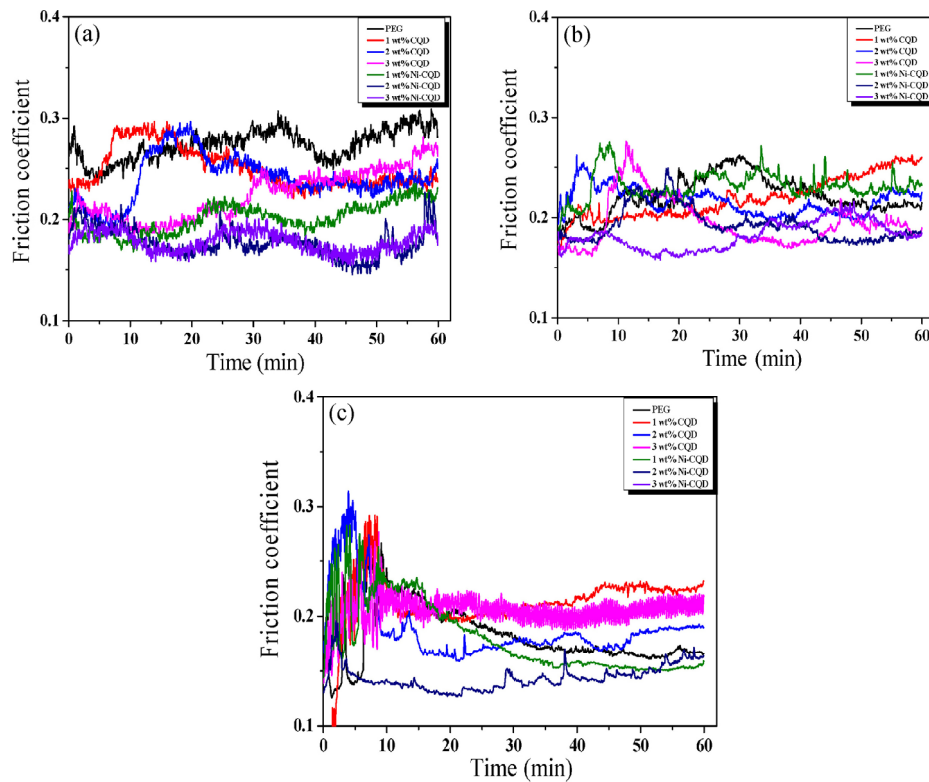


Fig. 5 Variation of friction coefficient as a function of the friction time at 25 mm/s for 60 min under the different loads: (a) 8 N; (b) 20 N; (c) 100 N.

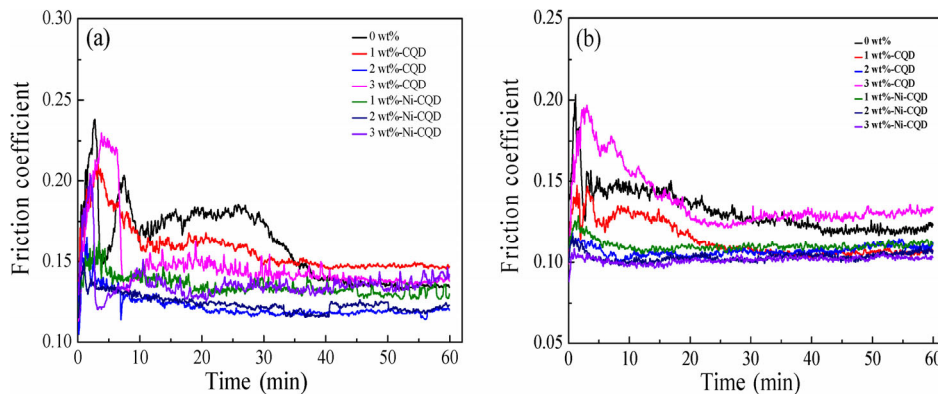


Fig. 6 Variation of friction coefficient as a function of the friction time under 100 N for 60 min at the different reciprocation speeds: (a) 17 mm/s; (b) 33 mm/s.

compared to those with pure PEG200. Therefore, we can conclude that the CQD and Ni-CQD particles play important roles in the wear resistance properties of PEG200.

3.4 Surface analysis

Table 1 shows optical images of the wear zones on the steel balls and disks lubricated with different oil samples under a load of 100 N with a reciprocation

speed of 25 mm/s over 60 min. The CQD particles did not enhance the lubrication properties of PEG200 under a load of 100 N. However, the wear scar diameters on the steel balls lubricated with PEG200 containing 1 wt%, 2 wt%, and 3 wt% Ni-CQDs were smaller than those on the balls lubricated with pure PEG200. The wear widths on the disks lubricated with PEG200 containing different amounts of Ni-CQD particles were also smaller than those on the disks lubricated with

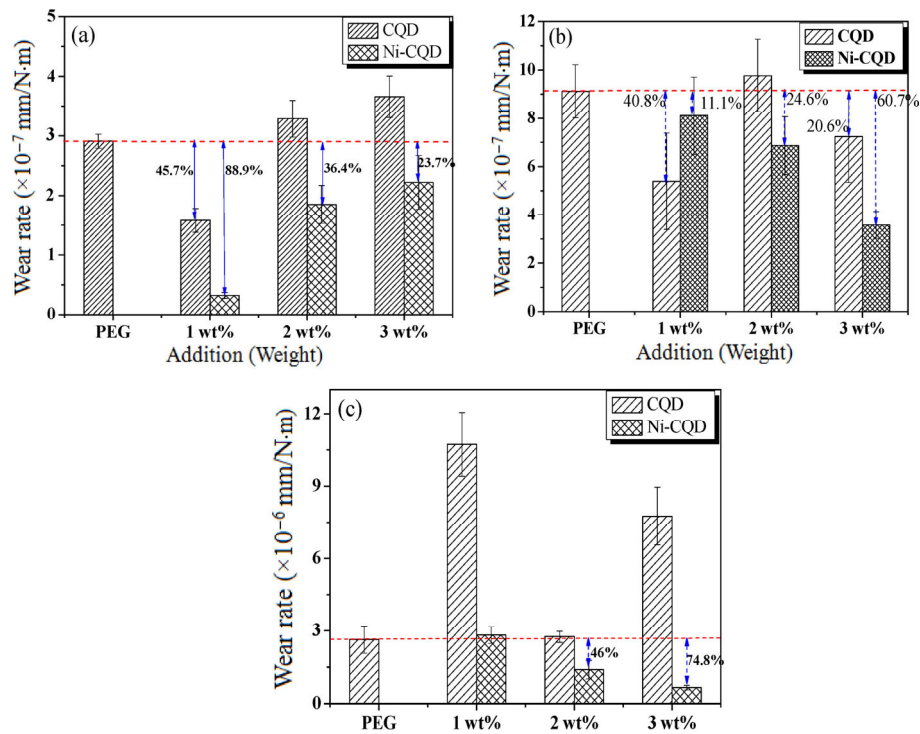


Fig. 7 Variations of wear rates of disks at 25 mm/s for 60 min under the different loads: (a) 8 N; (b) 20 N; and (c) 100 N.

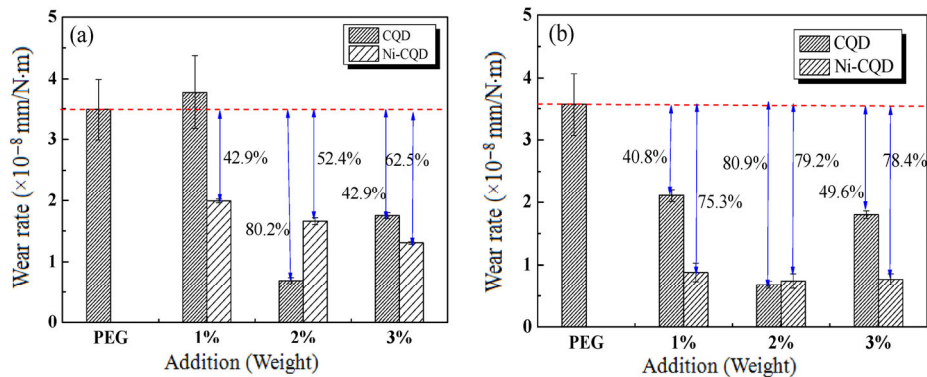


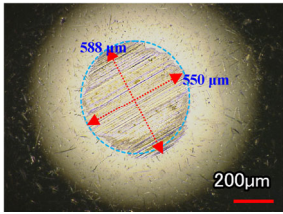
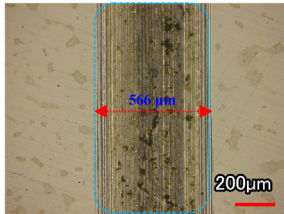
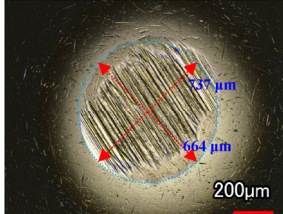
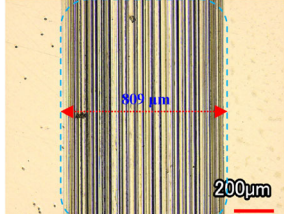
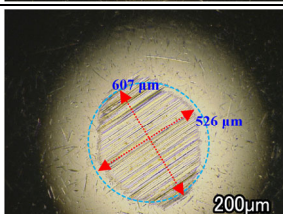
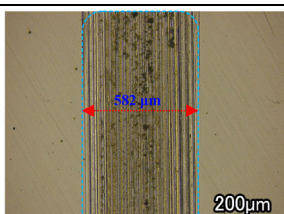
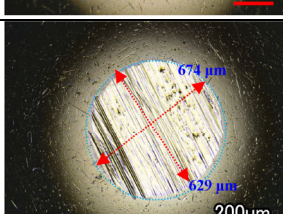
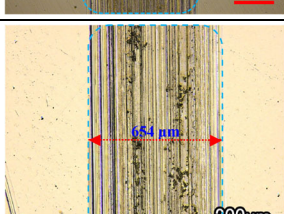
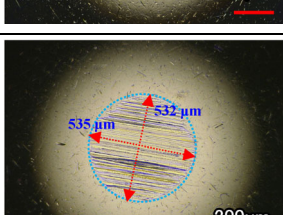
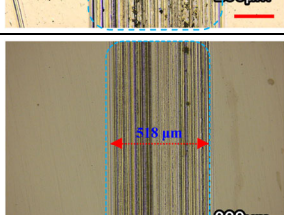
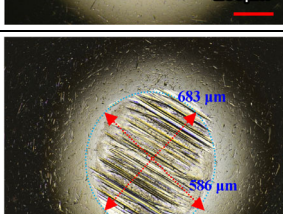
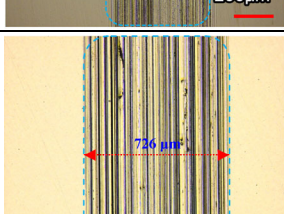
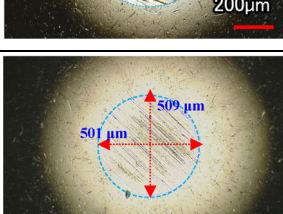
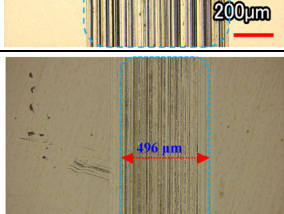
Fig. 8 Variations of wear rates of disks at 100 N for 60 min under the different reciprocation speeds: (a) 17 mm/s; (b) 33 mm/s.

PEG200 containing different amounts of CQD particles. The average wear width on the disks lubricated with PEG200 containing 3 wt% Ni-CQD decreased by 12.36% compared to that on the disks lubricated with pure PEG200. Overall, the Ni-CQD particles enhanced the wear resistance properties of PEG200 more than the CQD particles did.

Figure 9 shows SEM/EDS images of the wear zones on the disks lubricated with different oil samples. Exfoliation zones, furrows, and plastic deformation were observed on the surfaces of the steel balls lubricated with PEG200. These defects can be attributed to fatigue wear [37]. Significant wear occurred on the

surfaces of the disks lubricated with PEG200 containing different amounts of CQD particles and the number of furrows increased. The surfaces of the disks lubricated with PEG200 containing different amounts of Ni-CQD particles were also investigated. The furrows and exfoliation zones decreased slightly, which resulted in a smoother surface, when 2 wt% and 3 wt% Ni-CQD particles were added to the PEG200. Compared to the plain CQD particles, the Ni-CQD particles had a much greater effect on the lubrication properties of the PEG200. The EDS results revealed that Ni was present on the surfaces of the wear zones lubricated with PEG200 containing different amounts of Ni. The

Table 1 Optical images of wear zones lubricated with different oil samples at 100 N and 25 mm/s for 60 min.

Items	Steel ball	Disk	Change rate in wear width (%)
PEG			–
1 wt% CQD			–42.9
1 wt% Ni-CQD			–2.8
2 wt% CQD			–15.5
2 wt% Ni-CQD			8.4
3 wt% CQD			–28.26
3 wt% Ni-CQD			12.36

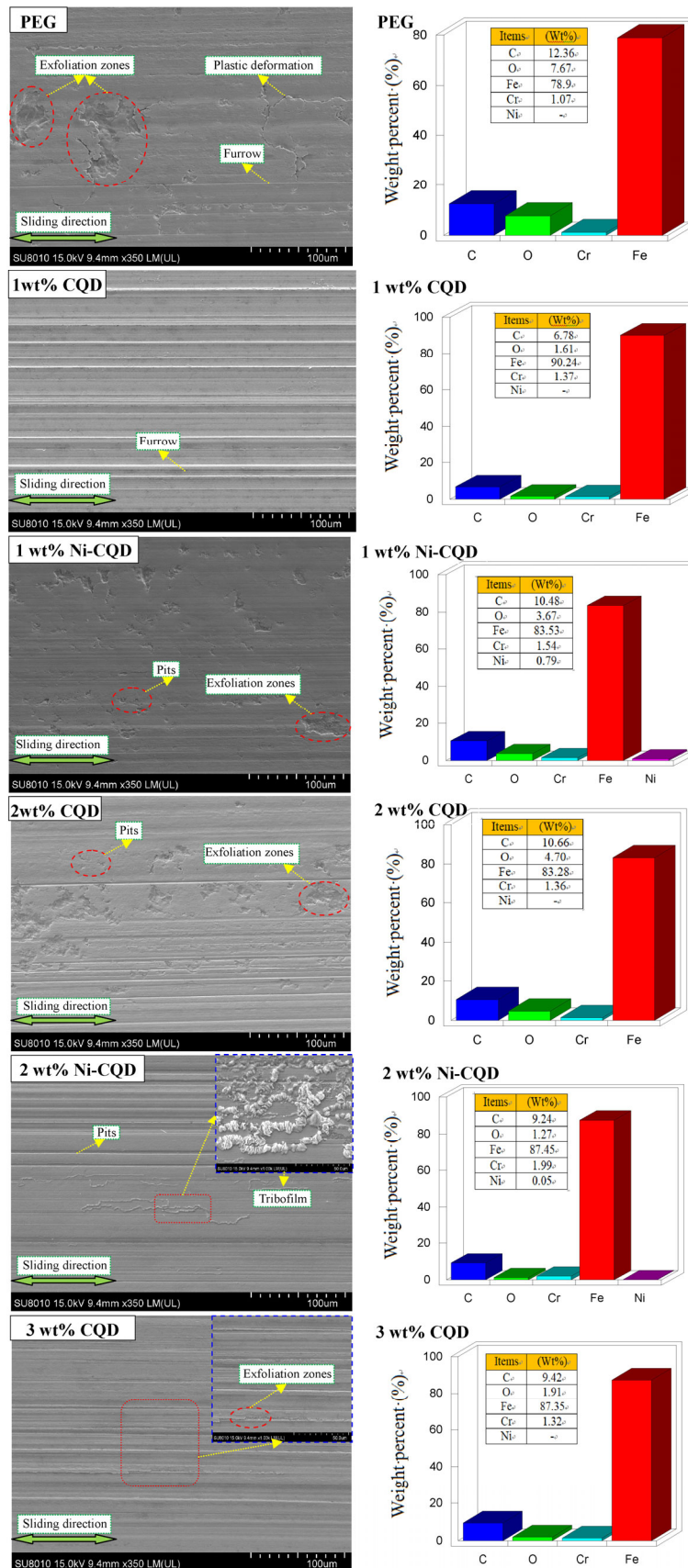


Fig. 9 SEM/EDS analysis of wear zones lubricated with different oil samples at 100 N and 25 mm/s for 60 min.

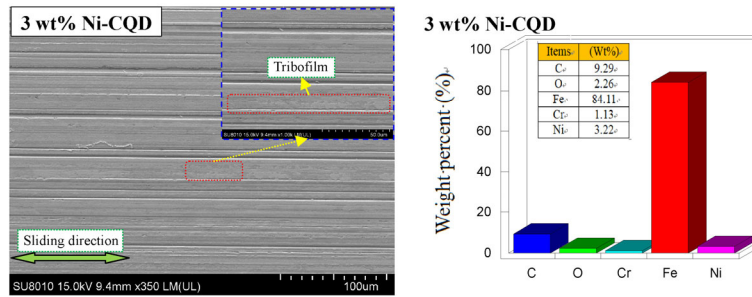


Fig. 9 (Continued)

weight percentages of Ni were 0.79 (1 wt% Ni-CQD), 0.05 (2 wt% Ni-CQD), and 3.22 (3 wt% Ni-CQD). Additionally, tribofilms formed on the surfaces when 2 wt% and 3 wt% Ni-CQD particles were added to the PEG200.

To determine if Ni-CQD particles can be used as a green lubricating additive in PEG200, the wear areas were also analyzed using a 3D software package, as shown in Fig. 10. The wear area was 2371.06 μm^2 for

pure PEG200. The wear areas of the disks increased by 307.2%, 4.34%, and 195% when lubricated with PEG200 containing 1 wt%, 2 wt%, and 3 wt% CQD particles, respectively, compared to that of the pure PEG200. For the Ni-CQD particles, the wear areas of the disks decreased by -7.1%, 46%, and 74.8% when 1 wt%, 2 wt%, and 3 wt% Ni-CQD particles were added, respectively. These results prove that Ni-CQD particles enhance the lubrication properties

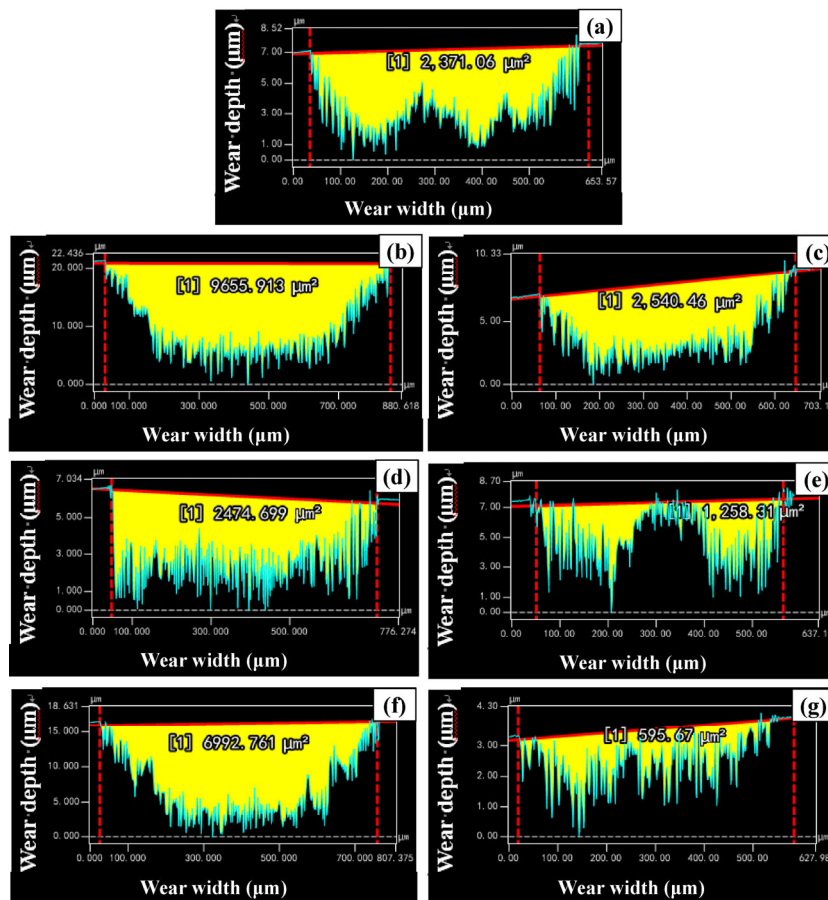


Fig. 10 Crossing areas of wear traces of disks lubricated with different oil samples at 100 N and 25 mm/s for 60 min. (a) PEG; (b) 1 wt% CQD; (c) 1 wt% Ni-CQD; (d) 2 wt% CQD; (e) 2 wt% Ni-CQD; (f) 3 wt% CQD; (g) 3 wt% Ni-CQD.

of PEG200 more than CQD particles do.

3.5 Friction and wear mechanism analysis

The CQD particles were able to modify the lubrication properties of the PEG200 at low loads and reciprocation speeds due to the large oil film thickness [40]. The small CQD particles entered the friction surface, resulting in a low average friction coefficient and wear rate during friction testing. The diameter of the Ni-CQD particles was smaller than that of the CQD particles after friction testing, as shown in Fig. 11 and Table 2.

For high loads and reciprocation speeds, the number of CQD particles entering into the friction surfaces of disks decreased due to the formation of a thin oil film and large shear force during friction testing [41]. Numerous furrows, pits, and exfoliation zones were created on the surfaces of the disks, resulting in abrasive wear during friction, as shown in Fig. 9.

The small Ni-CQD particles entered into the friction surface to participate in the formation of a tribofilm owing to the induced friction, which resulted in a smooth surface, as shown in Fig. 9. Characterization of the tribofilm was performed using XPS and Raman spectroscopy, which indicated that the Ni-CQD particles participated in the formation of lubrication films, which resulted in low friction coefficients and wear rates [35, 41]. XPS and Raman spectroscopy were

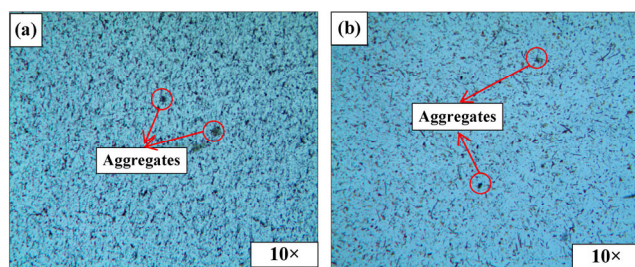


Fig. 11 Diameter distribution images of two kinds of Particles in PEG after friction. (a) CQD; (b) Ni-CQD.

Table 2 Diameter distribution range of two kinds of particles in PEG after friction.

Particle interval distribution (μm)	Quantity percentage (%)	
	CQD	Ni-CQD
0–5	82.3	87.8
5–15	17.2	12.1
≥ 15	0.45	0.029
Maximum particle area (μm^2)	520.74	185.35

used to verify the friction and wear mechanisms of CQD and Ni-CQD particles in PEG200. Figure 12 illustrates the variation in element chemical valence on the surfaces of wear zones lubricated with different oil samples. Figures 12(a), 12(b), and 12(c) illustrates the variation in chemical valence of the carbon element on the surfaces of the wear zones on the steel balls lubricated with different oil samples. The peaks at 284.6 eV, 286 eV, and 288.0 eV are attributed to C–C (or C–H), –C–O–, and –COOH groups, respectively [38]. The –C–O– and –COOH contents of the wear surfaces on the steel balls lubricated with PEG200 containing 2 wt% CQD, and PEG200 containing 2 wt% Ni-CQD, increased compared to those when using pure PEG200 for lubrication. These results are attributed to the CQD and Ni-CQD particles that took part in the formation of boundary lubrication films. Figures 12(d), 12(e), and 12(f) illustrates the variation in chemical valence of the O element on the wear surfaces of the steel balls lubricated with different oil samples. The peaks at 529.4 eV, 530.8 eV, and 532 eV are attributed to iron oxides, –OH, and FeOOH groups, respectively [38]. The –OH and FeOOH groups played an important role in forming the boundary lubrication films because the CQD and Ni-CQD particles participated in the formation of tribofilms and dehydrogenation of long-chain hydrocarbon molecules in the lubricating oils [42]. The FeOOH contents of the wear zones on the steel balls lubricated with PEG200 containing 2 wt% CQDs and Ni-CQDs were higher than those when using pure PEG200 for lubrication. Figure 12(g) illustrates the variation in the Fe element on the surfaces of the steel balls lubricated with different oil samples. The peak at 707 eV is attributed to Fe atoms. The peaks at 710.1 eV and 724.4 eV are attributed to $\text{Fe}_{1/2}$ and $\text{Fe}_{2/3}$, respectively. The peaks in the range of 709 eV–711 eV are attributed to iron oxides, such as FeO, Fe_2O_3 , and Fe_3O_4 . A peak at 707 eV (Fe atom) was detected on the surfaces of the wear zones lubricated with PEG200 containing 2 wt% CQDs and Ni-CQDs. These results indicate that a tribofilm can protect the base material, resulting in excited Fe atoms, low friction coefficients, and low wear rates. The results of Raman analysis also revealed differences between the tribofilms on the surfaces of the steel disks lubricated with different oil samples, as shown in Fig. 13. The

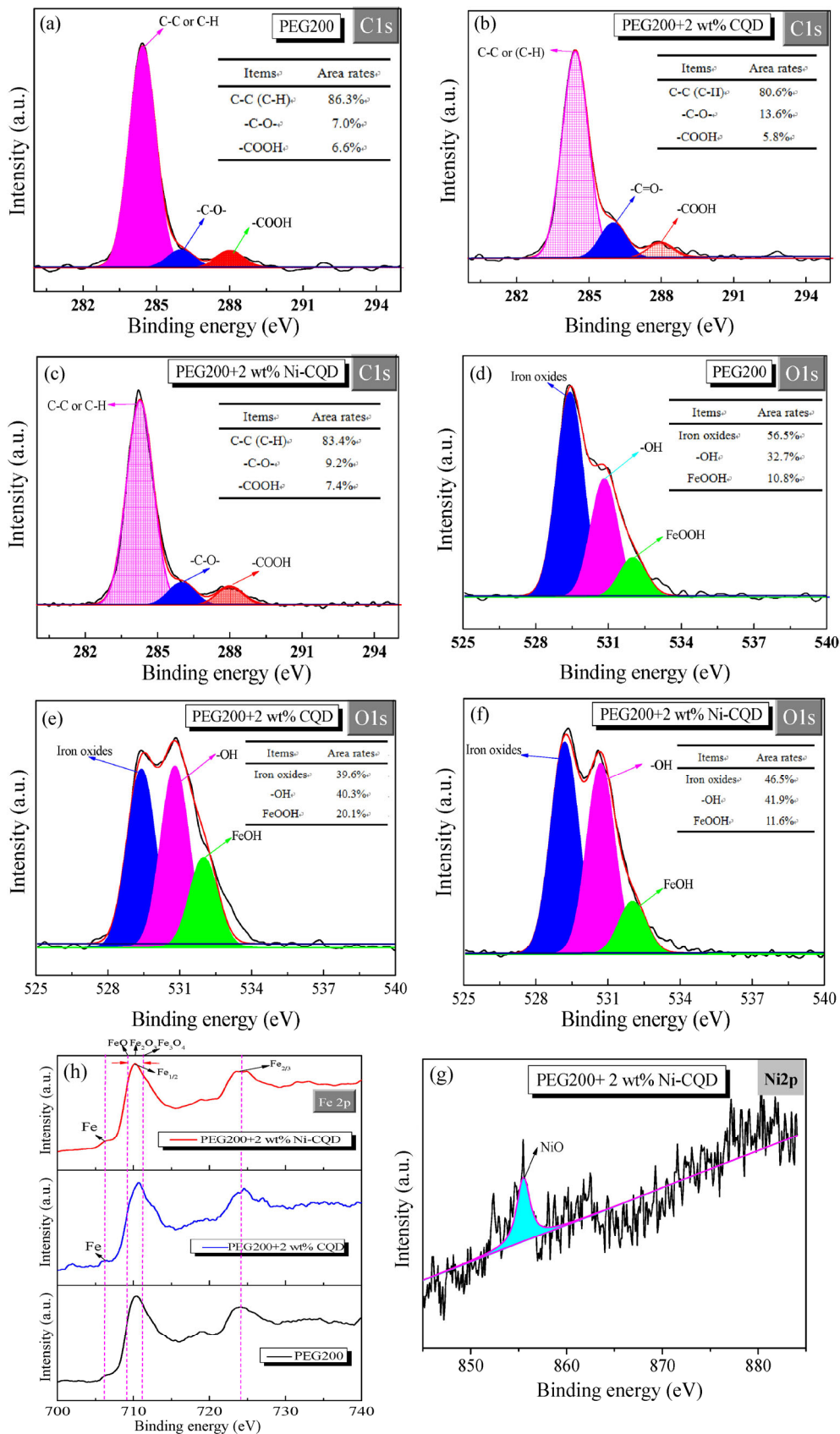


Fig. 12 C1s, O1s, Fe2p and Ni2p spectra of wear zones lubricated with different oil samples.

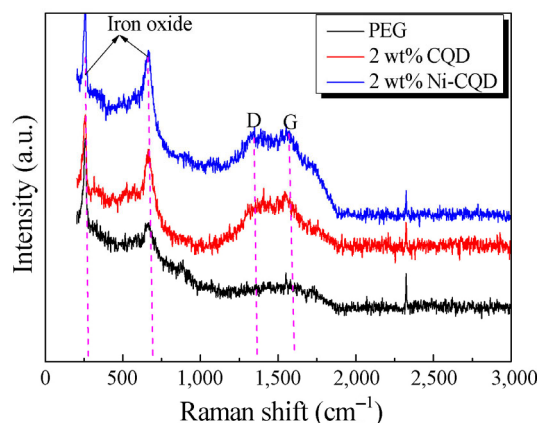


Fig. 13 Raman spectroscopy of wear zones lubricated with pure PEG200, PEG200+2 wt% CQD, and PEG200 + 2 wt% Ni-CQD particles.

peaks at 255 cm^{-1} and 672 cm^{-1} are attributed to iron oxides. The peaks at $1,350\text{ cm}^{-1}$ and $1,580\text{ cm}^{-1}$ correspond to the D and G peaks of carbon, respectively. Furthermore, the carbon contents on the surfaces of the wear zones lubricated with PEG200 containing 2 wt% CQD and 2 wt% Ni-CQD were higher than those on the surfaces lubricated with pure PEG200. The friction and wear mechanisms of CQD and Ni-CQD particles can be verified by referring to Fig. 14.

4 Conclusions

Ni-CQD particles were successfully prepared using a facile hydrothermal method. The effects of these particles on the lubrication properties of PEG200 were investigated using a reciprocating tribometer with

different loads and speeds. The results were compared to those of pure CQD particles. The following conclusions were obtained.

1) The APS values of the two nanomaterials were in the range of 5 nm–10 nm and they showed good dispersibility in PEG200.

2) Compared to the plain CQD particles, the Ni-CQD particles had a greater effect on the lubrication properties of PEG200.

3) Compared to PEG200 containing 2 wt% CQDs, the average friction coefficient and wear rate of PEG200 containing 2 wt% Ni-CQDs decreased by 35.5% and 36.4%, respectively, under a load of 8 N with a reciprocation speed of 25 mm/s.

4) Compared to PEG200 containing 3 wt% CQDs, the friction coefficient and wear rate of PEG200 containing 3 wt% Ni-CQDs decreased by 22% and 27%, respectively, under a load of 100 N with a reciprocation speed of 25 mm/s.

5) The friction and wear mechanisms of the Ni-CQDs were attributed to the fact that friction induced the Ni-CQDs to participate in the formation of a tribofilm, resulting in a low friction coefficient and wear rate.

Acknowledgements

The authors wish to express their gratitude to Mrs. Ziyang Lu and Mr. Lei Wang for their assistance with SEM/EDS and HRTEM testing. Financial support from the National Natural Science Foundation of China (Grant No. 51505121), Anhui University Outstanding

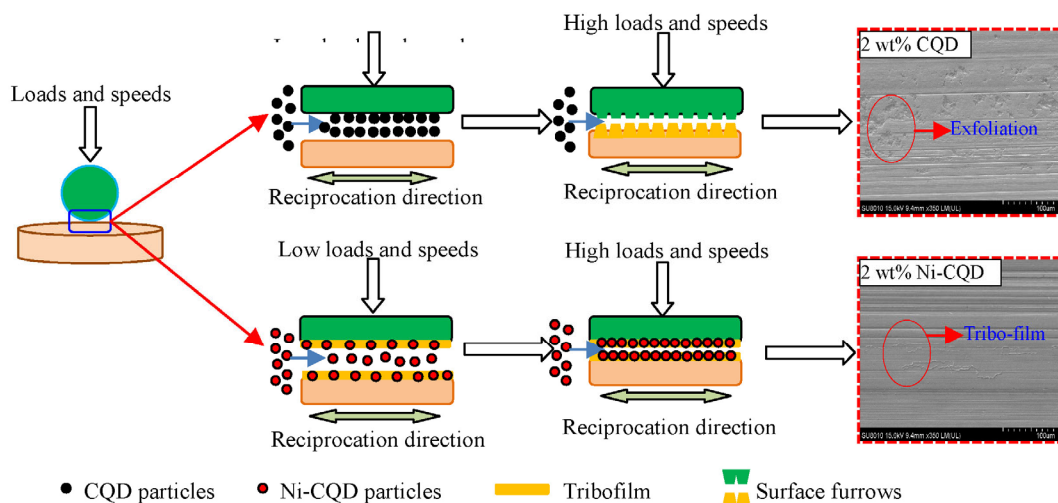


Fig. 14 Friction and wear mechanisms of CQD and Ni-CQD.

Young Talents Foreign Visiting and Training Program (gxgwfx 2018069), Anhui Provincial Natural Science Foundation (Grant Nos.1608085QE119), and Natural Science Foundation Project of the Anhui Education Committee (KJ2017A536) is gratefully acknowledged. Some of the experimental equipment used in this study in the Birmingham Centre for Cryogenic Energy Storage was obtained with support from the Engineering and Physical Sciences Research Council under the Eight Great Technologies: Energy Storage theme (EP/L017725/1).

Open Access This article is licensed under a Creative Commons Attribution 4.0 International License, which permits use, sharing, adaptation, distribution and reproduction in any medium or format, as long as you give appropriate credit to the original author(s) and the source, provide a link to the Creative Commons licence, and indicate if changes were made.

The images or other third party material in this article are included in the article's Creative Commons licence, unless indicated otherwise in a credit line to the material. If material is not included in the article's Creative Commons licence and your intended use is not permitted by statutory regulation or exceeds the permitted use, you will need to obtain permission directly from the copyright holder.

To view a copy of this licence, visit <http://creativecommons.org/licenses/by/4.0/>.

References

- [1] Erdemir A, Ramirez G, Eryilmaz O L, Narayanan B, Liao Y F, Kamath G, Sankaranarayanan S K R S. Carbon-based tribofilms from lubricating oils. *Nature* **536**(7614): 67–71 (2016)
- [2] Ewen J P, Heyes D M, Dini D. Advances in nonequilibrium molecular dynamics simulations of lubricants and additives. *Friction* **6**(4): 349–386 (2018)
- [3] Wong V W, Tung S C. Overview of automotive engine friction and reduction trends—Effects of surface, material, and lubricant-additive technologies. *Friction* **4**(1): 1–28 (2016)
- [4] Qu J, Barnhill W C, Luo H M, Meyer III H M, Leonard D N, Landauer A K, Kheireddin B, Gao H, Papke B L, Dai S. Synergistic effects between phosphonium-alkylphosphate ionic liquids and zinc dialkyldithiophosphate (ZDDP) as lubricant additives. *Adv Mater* **27**(32): 4767–4774 (2015)
- [5] Sharma V, Johansson J, Timmons R B, Prakash B, Aswath P B. Tribological interaction of plasma-functionalized polytetrafluoroethylene nanoparticles with ZDDP and ionic liquids. *Tribol Lett* **66**: 107 (2018)
- [6] Niste V B, Tanaka H, Sugimura J. The importance of temperature in generating ZDDP tribofilms efficient at preventing hydrogen permeation in rolling contacts. *Tribol Trans* **61**(5): 930–937 (2018)
- [7] Li X M, Rui M C, Song J Z, Shen Z H, Zeng H B. Carbon and graphene quantum dots for optoelectronic and energy devices: A Review. *Adv Funct Mater* **25**(31): 4929–4947 (2015)
- [8] Deepika, Li L H, Glushenkov A M, Hait S K, Hodgson P, Chen Y. High-efficient production of boron nitride nanosheets via an optimized ball milling process for lubrication in oil. *Sci Rep* **4**: 7288 (2014)
- [9] Gao W, Tkatchenko A. Sliding mechanisms in multilayered hexagonal boron nitride and graphene: The effects of directionality, thickness, and sliding constraints. *Phys Rev Lett* **114**(9): 096101 (2015)
- [10] Podgornik B, Kosec T, Kocijan A, Donik Č. Tribological behaviour and lubrication performance of hexagonal boron nitride (h-BN) as a replacement for graphite in aluminium forming. *Tribol Int* **81**: 267–275 (2015)
- [11] Kundu S, Sarojinjivee P, Karthick R, Anantharaj G, Saritha G, Bera R, Anandan S, Patra A, Ragupathy P, Selvaraj M, et al. Enhancing the efficiency of DSSCs by the modification of TiO₂ photoanodes using N, F and S, co-doped graphene quantum dots. *Electrochim Acta* **242**: 337–343 (2017)
- [12] Gong P W, Wang J Q, Hou K M, Yang Z G, Wang Z F, Liu Z, Han X X, Yang S R. Small but strong: The influence of fluorine atoms on formation and performance of graphene quantum dots using a gradient F-sacrifice strategy. *Carbon* **112**: 63–71 (2017)
- [13] Liang S S, Shen Z G, Yi M, Liu L, Zhang X J, Ma S L. In-situ exfoliated graphene for high-performance water-based lubricants. *Carbon* **96**: 1181–1190 (2016)
- [14] Zhang D W, Tian L, Guo H L. Preparation and optical properties of graphene quantum dots containing nitrogen. *J Inorg Mater* **31**(10): 1121–1128 (2016)
- [15] Gupta B, Kumar N, Panda K, Dash S, Tyagi A K. Energy efficient reduced graphene oxide additives: Mechanism of effective lubrication and antiwear properties. *Sci Rep* **6**: 18372 (2016)
- [16] Umrao S, Jang M H, Oh J H, Kim G, Sahoo S, Cho Y H, Srivastva A, Oh I K. Microwave bottom-up route for size-tunable and switchable photoluminescent graphene quantum dots using acetylacetone: New platform for enzyme-free detection of hydrogen peroxide. *Carbon* **81**: 514–524 (2015)

- [17] Berman D, Erdemir A, Sumant A V. Graphene: A new emerging lubricant. *Mater Today* **17**(1): 31–42 (2014)
- [18] Liang H Y, Bu Y F, Zhang J Y, Cao Z Y, Liang A M. Graphene oxide film as solid lubricant. *ACS Appl Mater Interfaces* **5**(13): 6369–6375 (2013)
- [19] Dong Y Q, Shao J W, Chen C Q, Li H, Wang R X, Chi Y W, Lin X M, Chen G N. Blue luminescent graphene quantum dots and graphene oxide prepared by tuning the carbonization degree of citric acid. *Carbon* **50**(12): 4738–4743 (2012)
- [20] Zhang W, Zhou M, Zhu H W, Tian Y, Wang K L, Wei J Q, Ji F, Li X, Li Z, Zhang P, et al. Tribological properties of oleic acid-modified graphene as lubricant oil additives. *J Phys D: Appl Phys* **44**(20): 205303 (2011)
- [21] Liu R L, Wu D Q, Feng X L, Müllen K. Bottom-up fabrication of photoluminescent graphene quantum dots with uniform morphology. *J Am Chem Soc* **133**(39): 15221–15223 (2011)
- [22] Gupta B, Panda K, Kumar N, Melvin A A, Dash S, Tyagi A K. Chemically grafted graphite nanosheets dispersed in poly(ethylene-glycol) by γ -radiolysis for enhanced lubrication. *RSC Adv* **5**(66): 53766–53775 (2015)
- [23] Shang W J, Cai T, Zhang Y X, Liu D, Liu S G. Facile one pot pyrolysis synthesis of carbon quantum dots and graphene oxide nanomaterials: All carbon hybrids as eco-environmental lubricants for low friction and remarkable wear-resistance. *Tribol Int* **118**: 373–380 (2018)
- [24] Ye Q H, Yan F Y, Luo Y M, Wang Y Y, Zhou X G, Chen L. Formation of N, S-codoped fluorescent carbon dots from biomass and their application for the selective detection of mercury and iron ion. *Spectrochim Acta Part A, Mol Biomol Spectrosc* **173**: 854–862 (2017)
- [25] Wang J, Qiu F X, Li X, Wu H Y, Xu J C, Niu X H, Pan J M, Zhang T, Yang D Y. A facile one-pot synthesis of fluorescent carbon dots from degrease cotton for the selective determination of chromium ions in water and soil samples. *J Lumin* **188**: 230–237 (2017)
- [26] Ma Y S, Cen Y, Sohail M, Xu G H, Wei F D, Shi M L, Xu X M, Song Y Y, Ma Y J, Hu Q. A ratiometric fluorescence universal platform based on N, Cu codoped carbon dots to detect metabolites participating in H₂O₂-generation reactions. *ACS Appl Mater Interfaces* **9**(38): 33011–33019 (2017)
- [27] Zhang Y X, Cai T, Shang W J, Liu D, Guo Q, Liu S G. Facile synthesis of photoluminescent inorganic-organic hybrid carbon dots codoped with B and N: Towards an efficient lubrication additive. *Dalton Trans* **46**(36): 12306–12312 (2017)
- [28] Ma W, Gong Z B, Gao K X, Qiang L, Zhang J Y, Yu S R. Superlubricity achieved by carbon quantum dots in ionic liquid. *Mater Lett* **195**: 220–223 (2017)
- [29] Wang B G, Tang W W, Lu H S, Huang Z Y. Ionic liquid capped carbon dots as a high-performance friction-reducing and antiwear additive for poly(ethylene glycol). *J Mater Chem A* **4**(19): 7257–7265 (2016)
- [30] Lei Y, Jiang J L, Bi T T, Du J F, Pang X J. Tribological behavior of in situ fabricated graphene–nickel matrix composites. *RSC Adv* **8**(39): 22113–22121 (2018)
- [31] Lei Y, Du J F, Pang X J, Wang H Z, Yang H, Jiang J L. Tribological properties and lubrication mechanism of *in situ* graphene-nickel matrix composite impregnated with lubricating oil. *Mater Res Express* **5**(5): 056512 (2018)
- [32] Jiang J L, He X X, Du J F, Pang X J, Yang H, Wei Z Q. In-situ fabrication of graphene-nickel matrix composites. *Mater Lett* **220**: 178–181 (2018)
- [33] Lei Y, Jiang J L, Bi T T, Wei Z Q. Effect of counterparts and applied load on the tribological behavior of the graphene-nickel matrix self-lubricating composite. *Tribol Lett* **66**(4): 129 (2018)
- [34] Yang J, Chen W L, Liu X P, Zhang Y, Bai Y. Hydrothermal synthesis and photoluminescent mechanistic investigation of highly fluorescent nitrogen doped carbon dots from amino acids. *Mater Res Bull* **89**: 26–32 (2017)
- [35] Hu E Z, Hu K H, Xu Z Y, Hu X G, Dearn K D, Xu Y, Xu Y F, Xu L. Investigation into the morphology, composition, structure and dry tribological behavior of rice husk ceramic particles. *Appl Surf Sci* **366**: 372–382 (2016)
- [36] Hu E Z, Hu X G, Liu T X, Liu Y M, Song R H, Chen Y Z. Investigation of morphology, structure and composition of biomass-oil soot particles. *Appl Surf Sci* **270**: 596–603 (2013)
- [37] Cheng L H, Yu D R, Hu E Z, Tang Y C, Hu K H, Dearn K D, Hu X G, Wang M. Surface modified rice husk ceramic particles as a functional additive: Improving the tribological behaviour of aluminium matrix composites. *Carbon Lett* **26**(1): 51–60 (2018)
- [38] Hu E Z, Xu Y F, Hu X G, Pan L J, Jiang S T. Corrosion behaviors of metals in biodiesel from rapeseed oil and methanol. *Renew Energy* **37**(1): 371–378 (2012)
- [39] Huang H, Hu H L, Qiao S, Bai L, Han M M, Liu Y, Kang Z H. Carbon quantum dot/CuS_x nanocomposites towards highly efficient lubrication and metal wear repair. *Nanoscale* **7**(26): 11321–11327 (2015)
- [40] Hu E Z, Hu X G, Liu T X, Fang L, Dearn K D, Xu H M. The role of soot particles in the tribological behavior of engine lubricating oils. *Wear* **304**(1–2): 152–161 (2013)
- [41] Hu E Z, Dearn K, Yang B X, Song R H, Xu Y F, Hu X G. Tribofilm formation and characterization of lubricating oils with biofuel soot and inorganic fluorides. *Tribol Int* **107**: 163–172 (2017)
- [42] Lin J, Wang Li, Chen G. Modification of graphene platelets and their tribological properties as a lubricant additive. *Tribol Lett* **41**: 209–215 (2011)



Zhiqiang TU. He received his bachelor degree in water supply and drainage science and engineering in 2017 from Binjiang College, Nanjing University of Information Technology,

Nanjing, China. After then, he was a master student in biological and environmental engineering at Hefei University. His research fields include biomass lubricant additives and biomass carbon quantum dot.



Enzhu HU. He received his master and Ph.D degrees in chemical engineering and environmental protection equipment and monitoring engineering from Hefei University of Technology, in 2011 and 2014, respectively. He joined the

Department of Chemical and Materials Engineering

at Hefei University from 2015. His current position is an associate professor and the director of the teaching and research Office. He is also a visiting scholar in Darmstadt University of Applied Science, Germany, in 2018. His research areas cover the tribology of biomaterials such as the nano fullerene and carbon quantum dots.